Optimal Control of Soft Robotic Crawlers Subject to Nonlinear Friction: A Perturbation Analysis Approach

Andrew Gusty, Cody Scarborough, Juncal Arbelaiz, Emily Jensen

***Abstract*— This letter considers the design of optimal open-loop control policies for a limbless, soft-robotic crawler subject to dry and viscous friction forces. The full dynamics of the crawler are modeled as a nonlinear wave equation, with a sliding friction force modeled as an asymmetric and nonlinear function that captures the effects of both wet and dry friction present in physical scenarios. A reduced-order model is formed utilizing perturbation method techniques. This reduced-order model is solved analytically and solutions are validated by comparison to numerical solutions for a soft-robotic crawler in a sewer pipe. This analytical solution is utilized to derive expressions for the resulting velocity, energy, mileage (efficiency), and engineering stress of a crawler. An optimal control design problem which maximizes velocity subject to mileage and stress constraints is formulated and solved numerically.**

I. Introduction

Soft robots have shown great promise for applications that require safe interaction with varying environments and people within them [1]. In particular, the motion of earthworms has inspired the design of soft-bodied, limbless robots – *peristaltic crawlers* – which have been proposed for the inspection and maintenance of narrow, long-distance pipes [2], [3], minimally invasive surgeries such as colonoscopies [4], or burrowing in subterranean environments [5].

In practical applications, peristaltic crawling may be limited by a relatively slow speed [6], energy inefficiencies [7], and limited on-board energy storage capacities. These challenges may become more pronounced with changes to the system or environment; e.g., the speed of peristaltic crawler is highly sensitive to the parameters of its actuator, such as actuation frequency and strength [6]. Controllers that optimize a robotic crawler for speed and efficiency, together with an understanding of relationships between actuator design and motion characteristics, can be leveraged to combat these challenges.

Experiments have shown that the motion of earthworms takes the form of traveling waves [8], [9]. This behavior has been modeled and the resulting speed and efficiency have been characterized analytically under linear conditions (assuming a linear, sliding friction force) [10]. Perturbation analysis was shown to provide insight into how speed and efficiency of the crawler are related to its actuator parameters.

A. Gusty is with the Department of Applied Mathematics, University of Colorado, Boulder (e-mail: andrew.gustyjr@colorado.edu). C. Scarborough and E. Jensen are with the Department of Electrical, Computer & Energy Engineering, University of Colorado, Boulder (e-mails: cody.scarborough@colorado.edu, ejensen@colorado.edu). J. Arbelaiz is with the Center for Statistics and Machine Learning and with the Princeton Neuroscience Institute, Princeton University (email: arbelaiz@princeton.edu)

However, crawlers in practical scenarios will encounter both dry and lubricated contacts, which have nonlinear friction effects and may significantly alter the worm's dynamics and resulting optimal control policies. Zimmerman [11] described the locomotion of earthworms under nonlinear, asymmetric frictional forces and found solutions numerically; Shen et al. [12] developed a hill-climbing algorithm for periodic control of a simple, two-section model of a peristaltic crawler. However, to the authors' knowledge, the equations of motion of such crawlers remain unsolved analytically when the nonlinear effects of dry friction is involved. Analytical solutions to the nonlinear dynamics of a crawler would provide precise relationships between controllable parameters and performance metrics, and enable the characterization of distinctly nonlinear effects on the system, such as stick-slip behavior.

The main result of this paper provides an analytical expression that describes the motion of a peristaltic crawler subject to a nonlinear friction force, consistent with a crawler in a wet environment where weak contact with dry or lubricated substrate may be encountered. We use a standard model for dry Coulomb friction [13]–[15], which is included as a perturbation in the form of an asymmetric signum function. Using this model, we derive an analytical relation between performance metrics such as speed, mechanical stress, and efficiency of a crawler and its actuation parameters, such as frequency, wavelength, and strength. We utilize these analytical relationships to formulate and solve an open-loop control problem to maximize the speed of a crawler while ensuring that it has enough energy storage to complete the intended goal and that the maximum stress at any point on the crawler does not exceed the ultimate tensile strength of its material.

We model the crawler using a nonlinear wave equation under physically relevant conditions where linear viscous friction forces dominate the dry nonlinear friction forces. We leverage perturbation theory with multiple time scales to obtain asymptotic approximations of solutions to the equation of motion. We compare these solutions to numerical results constructed using finite difference approximations to show the applicability of our analytical methods.

II. Problem Formulation

A. System Dynamics and Performance Metrics

We derive a continuous model of the motion of a soft-robotic crawler consistent with existing literature on peristaltic motion [8], [10], [16]. Analyzing the forces acting on

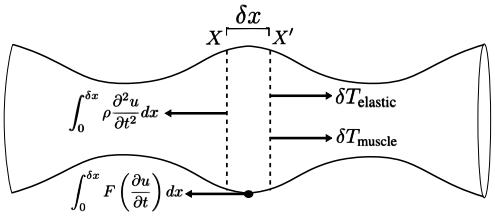

Fig. 1: Cross-sectional forces acting on a model of a limbless, earthworm-like crawler

a cross-section of a peristaltic crawler (Fig. 1) yields (see Appendix I),

$$A_c E \frac{\partial^2 u}{\partial x^2} + A_m \frac{\partial f(x,t)}{\partial x} = F_{\text{Fric}}\left(\frac{\partial u}{\partial t}\right) + \rho \frac{\partial^2 u}{\partial t^2}, \quad (1)$$

where $u(x,t)$ is the absolute displacement of the body of the crawler from its starting equilibrium position at location x and time t, $f(x,t)$ is a spatially and temporally periodic actuation force, $F_{\text{Fric}}(\frac{\partial u}{\partial t})$ is the friction force per unit length as a function of crawler velocity ($\frac{\partial u}{\partial t}$), A_c is the body's cross-sectional area, E is Young's modulus of elasticity of the body's material, A_m is the muscle's cross-sectional area, and ρ is the mass density of the crawler. The elastic and inertial forces (second-order spatial and temporal derivatives in (1)) suggest traveling wave solutions that will take on the spatial periodicity of the forcing term, f, and are damped by the nonlinear friction term $F_{\text{Fric}}(\frac{\partial u}{\partial t})$. We consider the crawler over the spatial domain $x \in [0, \lambda]$ ($x = 0$ is the tail and $x = \lambda$ is the head) with periodic boundary conditions, where λ is the wavelength of the periodic actuator, f, and let $t \in [0, \infty)$.

Variable	u	x	t	$A_c E$	ρ	A_m	f_0
Units	m	m	s	N	$\frac{\text{kg}}{\text{m}}$	m^2	N
Variable	ω	k	F_{Fric}	σ_s	V	P	M
Units	$\frac{1}{\text{s}}$	$\frac{1}{\text{m}}$	$\frac{\text{N}}{\text{m}}$	$\frac{\text{N}}{\text{m}^2}$	$\frac{\text{m}}{\text{s}}$	$\frac{\text{Nm}}{\text{s}}$	$\frac{\text{m}}{\text{J}}$

TABLE I: Units of parameters and performance metrics in crawler dynamics.

In practical settings, a crawler is constrained by metrics such as speed, efficiency, and durability. We define these metrics in relation to the forcing function, $f(x,t)$, which models the traveling elongation/contraction waves which occur in the movement of earthworms [8], [17], [18]. Robotic crawlers commonly emulate these contractions through sequential activation of pneumatic artificial muscle or servo motor components along the body of the crawler [2]–[5], [9]. A simple continuum model which describes this behavior is,

$$A_m f(x,t) = f_0 \sin(kx - \omega t), \quad (2)$$

where $f_0 = e_0 A_m$ and e_0 is the amplitude of the muscle stress or a modulus of elasticity (units of N/m^2), k is the actuator's wave number ($k = 2\pi/\lambda$, λ is the wavelength of contractions) and ω is the frequency of contractions (rad/s). The left-hand side of (1) represents in the internal tension per unit length of the crawler,

$$\frac{\partial}{\partial x} T_{\text{Internal}} := A_c E \frac{\partial}{\partial x}\left(\frac{\partial u}{\partial x} + \frac{f_0}{A_c E}\sin(kx - \omega t)\right) \quad (3)$$

This tension, $T_{\text{Internal}} = A_c E u_x + f$ (where $u_{(\cdot)}$ denotes the partial derivative w.r.t. $(\cdot)$), results from the sum of the actual crawler strain, u_x and the instantaneous strain provided by the actuator, $(1/A_c E) \cdot f(x,t)$ [10]. This gives rise to an expression for the maximum *engineering stress* on the crawler,

$$\sigma_s = \frac{T_{\max}}{A_c} \quad , \quad T_{\max} = \sup_{x \in [0,\lambda],\, t \in [0, \frac{1}{\omega}]} T_{\text{Internal}}(x,t), \quad (4)$$

where σ_s denotes the maximum engineering stress and $T_{\max}$ is the maximum internal tension on the crawler.[1]

As the crawler operates, it will exhibit net movement in a desired direction. The speed, V, at which the crawler moves in this direction as a whole is the instantaneous velocity of the crawler, u_t, averaged over its wavelength ($\lambda = \frac{2\pi}{k}$),

$$V = \frac{1}{\lambda}\int_0^{\lambda} u_t(x,t)dx. \quad (5)$$

Our metric for energy consumption relies on the elastic potential energy of the system, PE, over the wavelength of the crawler:

$$PE = \frac{1}{2} A_c E \int_0^{\lambda} \left(u_x + \frac{1}{A_c E} f(x,t)\right)^2 dx. \quad (6)$$

PE remains constant due to the periodicity of the actuator and u_x. Equation (6) is physically analogous to integrating the potential energy density of a distributed spring system with spring constant $A_c E$. The actuator inputs potential energy into the system by modifying the effective strain, $(u_x + \frac{1}{A_c E} f)$. Thus, the power input to the system, P, is

$$P = \int_0^{\lambda} \left(u_x + \frac{1}{A_c E} f\right)(f_t)\, dx, \quad (7)$$

which can be derived by taking the time derivative of (6) and applying partial integration to derive an equation for the power balance of the system [10]. The quotient of (5) divided by (7) gives the net distance that the crawler can move per unit of energy - a *mileage quantity*, M with units (m J^{-1}):

$$M \equiv \frac{|V|}{P}. \quad (8)$$

B. Weakly Nonlinear Friction

Dry friction plays a critical role both theoretically and experimentally in generating net motion in earthworms and peristaltic crawlers [2]–[5], [9]–[12]. However, the dynamics of a crawler subject to dry friction remain unsolved due to the nonlinear nature of dry friction force. In the case of a dry or lubricated substrate, Stribeck or Coulomb friction models [15] are commonly used, while in a fully wet environment, viscous friction can be modeled linearly with respect to sliding speed. Each of these models are shown in Fig. 2.

[1]We model the crawler with a constant cross-section, A_c, which is why we measure engineering stress instead of true stress. However, in most physical crawlers, the cross sectional area will be somewhat smaller in the elongated portions of the crawlers body, meaning that it may be necessary to estimate the minimum cross sectional area of the crawler in its most elongated position.

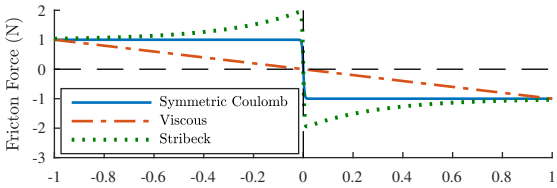

Fig. 2: Common models for sliding friction forces encountered by a limbless crawler

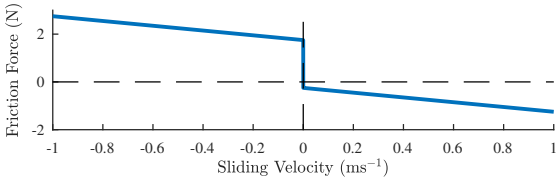

Fig. 3: Asymmetric Coulomb-Viscous dry friction model ($\epsilon = 1$)

Since crawlers may encounter both viscous and dry friction effects, we use a dry Coulomb friction model with an added viscous term. To realize a preferential direction of motion, a crawler must break symmetry through anisotropic friction [10] [18], which is commonly achieved by a mechanical scheme in which the friction coefficient is lower during forward sliding than during backward sliding [5], [17], [19]. Asymmetry is incorporated into the Coulomb-Viscous friction model by shifting the friction force curve downwards (Fig. 3). The asymmetric model is given by,

$$F(u_t) = c_v u_t + \epsilon c_d(\text{sgn}(u_t) - n_F), \tag{9}$$

where $c_d = \rho g$ (g is acceleration due to gravity) is the normal force per unit length on the substrate, $c_v > 0$ is the coefficient of viscous friction ($c_v = \eta A_c/d$, where η is dynamic viscosity of the fluid and d is the gap distance between the crawler and the substrate), u_t is the instantaneous velocity at a point on the crawler, ϵ is the coefficient of dry sliding friction, and $0 \leq n_F \leq 1$ represents a downward shift to bring about asymmetry of the friction force between positive and negative velocity. To employ perturbation theory, we assume an environment in which the coefficient of dry sliding friction is small ($\epsilon \ll 1$), which is true for many materials used in the construction of pipes as well as in colonoscopies which use lubricant to reduce dry friction. We also show that even for $\epsilon = 1$, our perturbation solution still shows strong agreement with the numerical solution to the dynamics for the selected parameters.

C. Open-Loop Control Problem

Selection of forcing frequency (ω), wave number (k), and strength (f_0) to maximize the speed of the crawler is formulated as an optimal open-loop control problem. Constraints on the system's energy storage capability and the ultimate tensile strength of its material are incorporated, leading to the constrained problem,

$$\max_{\omega,k,f_0} \quad V(\omega,k,f_0) \tag{10}$$

$$\text{subject to} \quad \text{M}(\omega,k,f_0) \geq \frac{D}{J_0}, \tag{11}$$

$$\sigma_s(\omega,k,f_0) \leq \sigma_{\max}, \tag{12}$$

where $V(\omega,k,f_0)$ is the net velocity of the crawler, $M(\omega,k,f_0)$ is the mileage of the crawler, D is the distance required by the task goal, J_0 is the total energy which the crawler can store, $\sigma_s(\omega,k,f_0)$ is the mechanical stress on the worm's material at its most elongated position, and $\sigma_{\max}$ is the ultimate tensile strength of the crawler material. The solution to this problem can provide, a control policy that ensures completion of a task like navigation of a sewer pipe as quickly as possible under energy constraints and without damage to the system.

III. Analysis of Nonlinear Crawler Dynamics

A. Non-dimensional Dynamics

We non-dimensionalize the dynamics of (1) to reduce the number of parameters and emphasize their respective impacts on system metrics. We set the characteristic time-scale $t_c = \frac{1}{\omega_n}$, where $\omega_n = k\sqrt{\frac{A_c E}{\rho}}$ is the undamped natural frequency of (1), and set the characteristic length scale $x_c = \frac{1}{k}$, where k is the wave number of the nonhomogeneous forcing term given in (2). Finally, we scale $u(x,t)$ by the characteristic displacement $u_c = \frac{f_0}{kA_cE} = \frac{f_0 k}{\rho\omega_n^2}$ and introduce the following non-dimensional variables,

$$\tau = \omega_n t, \quad \chi = kx, \quad \mu = u\frac{kA_cE}{f_0}. \tag{13}$$

Substituting (13) into (1) gives the non-dimensional dynamics

$$\mu_{\chi\chi} - \mu_{\tau\tau} - \zeta\mu_\tau + \epsilon\pi_r(\text{sgn}(\mu_\tau) - n_F) = cos(\chi - \alpha\tau) \tag{14}$$

where $\alpha = \frac{\omega}{\omega_n}$ is dimensionless and the dimensionless groups ζ and π_r are given by

$$\zeta = \frac{c_v}{k\sqrt{\rho A_c E}}, \quad \pi_r = \frac{c_d}{f_0 k}. \tag{15}$$

ζ is analogous to a *damping ratio*. In the remainder of this section, we utilize perturbation theory to obtain an analytical expression for a well-ordered expansion $\tilde{\mu}$ of the form

$$\tilde{\mu}(\chi,\tau) := \tilde{\mu}^{(0)}(\chi,\tau) + \epsilon\tilde{\mu}^{(1)}(\chi,\tau) \approx \mu(\chi,\tau), \tag{16}$$

which approximations a solution μ of (14). We begin by introducing some preliminaries.

B. Perturbation Analysis

Definition 1: The functions $\theta^{(0)}, \theta^{(1)}, \ldots$ are *well-ordered* or form as *asymptotic sequence* as $\epsilon \to 0$ iff $\theta^{(n)} = o(\theta^{(m)})$ as $\epsilon \to 0$ for all m and n such that $m < n$. If $\theta^{(0)}, \theta^{(1)}, \ldots$ form an asymptotic sequence, then $\theta(\epsilon)$ has an *asymptotic expansion* to n terms with respect to this sequence [20], iff

$$\theta = \sum_{k=0}^{n} a_k\theta^{(k)}(\epsilon) + o(\theta^{(n)}) \text{ as } \epsilon \to 0. \tag{17}$$

Since the higher order terms are dominated by the lower order terms, $\theta^{(k)}$ can be solved for independently of $\theta^{(m)}$ for $k < m$. Any term which violates the well-orderedness of an asymptotic expansion is called a *secular term*, and makes the problem a *singular perturbation problem*. In these cases, we employ the following well-known result [21]:

Lemma 1: A solution u for a nonhomogeneous equation of the form

$$\mathcal{L}u(x,t) = f(x,t), \tag{18}$$

for $\mathcal{L}$ a linear differential operator, exists and remains well-ordered if and only if f is orthogonal to the null space of the adjoint operator $\mathcal{L}^\dagger$ [21]. This condition is called a *solvability condition*.

The perturbation problem in (14) is singular due to the asymmetry in the dry friction force caused by the downward shift of n_F. This will result in the crawler's non-dimensional displacement, μ, slowly growing over time as a preferential direction of motion and net velocity is achieved, while it oscillates back-and-forth over shorter time-scales, leading to a singular term. Because of this "slow" and "fast" behavior in the dynamics, we introduce two non-dimensional time-scales, which can be assumed to be independent of each other for ϵ sufficiently small [21], as a means to enforce the solvability condition of Lemma 1:

$$\tau_1 = \tau, \quad \tau_2 = \epsilon\tau. \tag{19}$$

This modifies the derivative operator with respect to τ:

$$\partial_\tau = \partial_{\tau_1} + \epsilon\partial_{\tau_2}\ , \quad \partial_{\tau\tau} = \partial_{\tau_1\tau_1} + 2\epsilon\partial_{\tau_1\tau_2} + \epsilon^2\partial_{\tau_2\tau_2}. \tag{20}$$

Assuming an asymptotic expansion for $\mu(\chi,\tau_1,\tau_2)$ exists,

$$\mu(\chi,\tau) = \mu^{(0)}(\chi,\tau_1,\tau_2) + \epsilon\mu^{(1)}(\chi,\tau_1,\tau_2) + \dots \tag{21}$$

where $\mu^{(0)} = O(1)$ is referred to as the 0^{th}-order term and $\mu^{(1)} = O(\epsilon)$ is the 1^{st}-order term. The first two terms of (21) are the solutions to the following system of PDEs over the interval $\chi \in [0, 2\pi]$ with periodic boundary conditions:

$$\mathcal{L}\mu^{(0)} = \cos(\chi - \alpha\tau_1) \tag{22}$$

$$\mathcal{L}\mu^{(1)} = \zeta\mu^{(0)}_{\tau_2} + 2\mu^{(0)}_{\tau_1\tau_2} + \pi_r(\text{sgn}(\mu_\tau) - n_F) \tag{23}$$

$$\mathcal{L} = (\partial_{\chi\chi} - \partial_{\tau_1\tau_1} - \zeta\partial_{\tau_1}). \tag{24}$$

This system can be verified by substituting (21) into (14) and matching orders of magnitude $(O(1), O(\epsilon), ..)$ to generate the above system of PDEs.

We demonstrate numerically that the expansion, $\tilde{\mu}^{(0)} + \epsilon\tilde{\mu}^{(1)}$ that solves the following system of linear PDEs over $\chi \in [0, 2\pi]$ with periodic boundary conditions,

$$\mathcal{L}\tilde{\mu}^{(0)} = \cos(\chi - \alpha\tau_1) \tag{25}$$

$$\mathcal{L}\tilde{\mu}^{(1)} = \zeta\mu^{(0)}_{\tau_2} + 2\mu^{(0)}_{\tau_1\tau_2} + \pi_r(\text{sgn}(\mu^{(0)}_\tau) - n_F), \tag{26}$$

provides a quite accurate approximation of $\mu^{(0)} + \epsilon\mu^{(1)}$. We obtain $\tilde{\mu}^{(0)}$ and $\tilde{\mu}^{(1)}$ analytically, as stated next.

Proposition 1: The solutions $\tilde{\mu}^{(0)}$ and $\tilde{\mu}^{(1)}$ to the PDEs (25) and (26) are

$$\tilde{\mu}^{(0)}(\chi,\tau_1,\tau_2) = R_0\cos(\chi - \alpha\tau_1 - \phi_0) + C_1\tau_2, \tag{27}$$

$$\tilde{\mu}^{(1)}(\chi,\tau_1) = \sum_{n=1}^{\infty} R_n\cos(n(\chi - \alpha\tau_1 - \phi_0) - \phi_n), \tag{28}$$

where

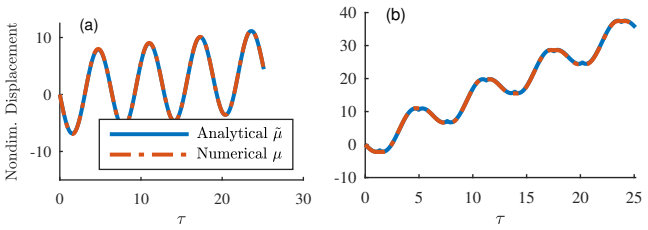

Fig. 4: Numerical solution to the full system dynamics in (14) vs. approximate analytic solution calculated in Section III-B for the tail of a peristaltic crawler under (a) weakly nonlinear friction ($\epsilon = 0.1$) and (b) nonlinear friction ($\epsilon = 1$)

$$R_0 = \frac{1}{\sqrt{(\alpha^2-1)^2+(\zeta\alpha)^2}},\quad R_n = \sqrt{\frac{a_n^2+b_n^2}{n^4(\alpha^2-1)^2+(\zeta\alpha n)^2}}$$
$$\phi_0 = \tan^{-1}\left(\frac{\zeta\alpha}{\alpha^2-1}\right),\ \phi_n = \tan^{-1}\left(\frac{b_n n^2(\alpha^2-1)+a_n\zeta\alpha n}{a_n n^2(\alpha^2-1)-b_n\zeta\alpha n}\right) \tag{29}$$

and $C_1 \approx \frac{\pi_r}{\zeta}(n_F - \frac{2\gamma}{\pi})$ is an arbitrary constant selected to satisfy the solvability condition for (26). The values of a_n and b_n describe the effective driving function which generates the first order update, $\tilde{\mu}^{(1)}$, and are provided in Appendix II along with γ.

The proof of Proposition 1 is provided in Appendix II. Summarizing, we approximate $\mu(\chi,\tau)$ using the well-ordered expansion (16) where $\tilde{\mu}^{(0)}$ and $\tilde{\mu}^{(1)}$ are given in (27) and (28), respectively.

C. Numerical Validation

To determine accuracy of $\tilde{\mu}$ (16), we compare it to the numerical solution of the full system dynamics in (14) solved using finite difference approximations. For physically relevant conditions, we choose parameter values for an earthworm crawler inside a sewer pipe [2] [3], setting $A_c = A_m = 10^{-4}$m (1 cm^2 cross-section), $\rho = (10^3\,\text{kg/m}^3)\cdot A_c = 0.1$ kg/m (density of water), $E = 140$ kPa (Young's Modulus of an earthworm [22]), $c_v = \eta A_c/d = 1$ (where $\eta \approx 1$ is the dynamic-viscosity of water and $d = 10^{-4}$m is the gap distance between crawler and substrate), $c_d = \rho g \approx 1$ (where g is acceleration due to gravity), $\epsilon = 0.1$ (approximate coefficient of sliding friction for cast iron), and $e_o = 5$ kPa.

Fig. 4 shows strong agreement between the multiple scales and numerical solutions to the non-dimensional system dynamics. For $\epsilon << 1$, the solutions are close to slowly drifting sinusoids, with the multiple scales and numerical solutions being virtually indistinguishable. As $\epsilon \to 1$, indicating a dryer substrate with stronger nonlinear effects, the peaks of the sinusoids are flattened, which is a well-known effect in systems with dry friction known as *stick-slip* [15]. For the presented physical parameters, we note that there is still strong agreement between the numerical and analytic solutions for $\epsilon = 1$ demonstrating the applicability of perturbation methods to analyze peristaltic motion. Future work will determine what parameter values are required for our approximation to hold as $\epsilon \to 1$.

IV. Analysis of Performance Metrics

Using the asymptotic expansion calculated in the previous section, we calculate the maximum engineering stress, speed,

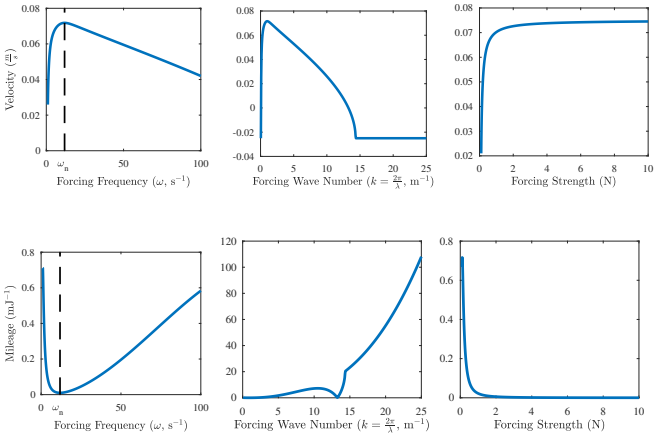

Fig. 5: Velocity and mileage estimates based on (31) for (33) a limbless crawler with respect to actuator frequency (ω), wave number (k), and strength (f_0).

power, and mileage of the crawler using the formulations provided in (4), (5), (7), and (8) respectively,

$$\sigma_s \approx \frac{f_0}{A_c E} R_0 \alpha \sqrt{1 + \left(\frac{c_v}{\rho \omega_n}\right)^2} \tag{30}$$

$$V \approx \frac{\epsilon c_d}{c_v}\left(n_F - \frac{2\gamma}{\pi}\right), \quad \gamma = \sin^{-1}\left(\frac{\epsilon C_0}{R_0 \alpha}\right) \tag{31}$$

$$P \approx \frac{\pi R_0 f_0^2 \omega \sin(\phi_0)}{k A_c E} \tag{32}$$

$$M \approx \frac{\epsilon c_d k A_c E}{\pi \omega f_0^2 R_0 \sin(\phi_0) c_v}\left|n_F - \frac{2\gamma}{\pi}\right| \tag{33}$$

As f_0 increases, the velocity and mileage increase and decrease respectively, with both relationships saturating quickly. At resonance forcing frequency ($\alpha = 1$), the velocity and engineering stress of the system are each maximized while the mileage is minimized. This agrees with previous work on a discrete models of similar crawlers that forcing at mechanical resonance leads to optimal velocity [12], and implies that there will be a trade-off between crawler speed, mileage, and stress in the control policy for a peristaltic crawler. At resonance, the velocity of the system is

$$V^* \approx \frac{\epsilon c_d}{c_v}\left(n_F - \frac{2\sin^{-1}(\epsilon \pi_r n_F)}{\pi}\right). \tag{34}$$

The relationship between the velocity, mileage, and actuation parameters f_0, ω, and k are shown in Fig. 5.

V. Optimal Control Policy

We now solve the control problem presented in Section II-C, to obtain an open-loop control policy for the actuation frequency (ω), wave number (k), and strength (f_0) which maximize the velocity of the crawler subject to physical constraints. The solution to the unconstrained problem: $\max_{\omega, f_0} \; V(\omega, f_0)$ is achieved at $\omega = \omega_n$ and $f_0 \to \infty$ and follows from the analysis presented in Section IV.

We solve the constrained problem using a grid search over ω and k, with f_0 chosen to enforce feasibility at each point in the ω-k plane, $(\bar{\omega}, \bar{k})$. We leverage analytical expressions

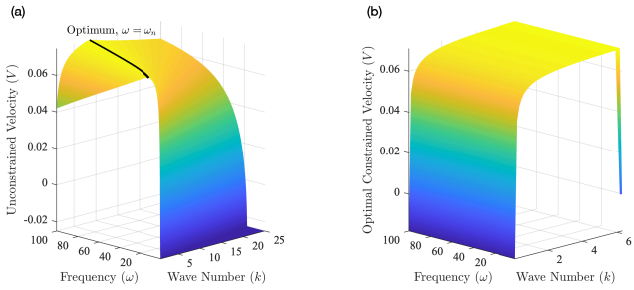

Fig. 6: 3-D Surface plot of the (a) net unconstrained velocity and (b) optimal constrained velocity of a continuous crawler with respect to its actuator frequency and wave number.

for the constraints and objective function in Section IV to derive a constraint for f_0 given fixed $\bar{\omega}$ and $\bar{k}$.

$$\text{Mileage Constraint: } f_1 := \left\{f_0;\ M - \tfrac{J_0}{D} = 0\right\} \tag{35}$$

$$\text{Stress Constraint: } f_0 \leq \frac{\sigma_{\max} A_c E}{R_0 \alpha \sqrt{1 + \left(\frac{c_v}{\rho \omega_n}\right)^2}} := f_2 \tag{36}$$

$$\implies \bar{f}_0 = \min\{f_1, f_2\} \tag{37}$$

Since the velocity V and mileage M are monotonically increasing and decreasing, respectively with f_0, we replace inequality (11) with equality (35). We solve (35) numerically using Matlab's `fzero()` function and calculate $V(\bar{\omega}, \bar{k}, \bar{f}_0)$. Computations are repeated over the $\omega - \kappa$ grid with the largest velocity recorded as optimal.

Plots of the velocity for the unconstrained and constrained optimization problem are given in Fig. 6, where we use the same constants as Section III-C, except that ω, k, and f_0 are free variables (we fix $f_0 = 1.5$ for the unconstrained velocity). To illustrate the results of the method, we choose $D = 1$ m, $J_0 = 20$ J, and $\sigma_{\max} = 100$ kPa. For the unconstrained problem, the optimal velocity occurs on the black line in Fig. 6-(a), which is at resonant forcing. This indicates that *an unconstrained crawler should be forced at mechanical resonance to achieve optimal velocity*. However, *for the constrained problem, the optimal velocity is dependent on k rather than ω*, which indicates that improving the velocity through ω requires the use of a worse f_0 to ensure feasibility and vice-versa, so that the optimal constrained velocity is ultimately determined by k.

VI. Conclusion

In this letter, we derived an optimal open-loop control policy for a peristaltic crawling robot subject to both viscous and dry friction effects. Using perturbation theory, we constructed asymptotic solutions to the crawler's dynamics, which show strong agreement with numerical solutions to the same system. These solutions were used to form analytical expressions for performance metrics such as stress, velocity, and mileage of a crawler. Using these metrics, we showed that there is substantial trade-off between mileage, stress, and velocity of a crawler, which motivates a constrained optimization problem to maximize the speed of a crawler while ensuring that it has enough energy to complete its required task and that the internal stress does not exceed the ultimate

tensile strength of the crawler's material. Future work entails developing optimal feedback control of a crawler subject to environmental disturbances and more complex boundary conditions. Comparisons between distributed and centralized control policies may also be made to compare the roles of local proprioception and sensory feedback to centralized feedback for maintaining optimal periodic locomotion patterns in biological and robotic systems.

REFERENCES

[1] M. Hammond, V. Cichella, and C. Lamuta, "Bioinspired soft robotics: State of the art, challenges, and future directions," *Curr. Robot. Rep.*, vol. 4, pp. 65–80, 2023.

[2] T. Tanaka, K. Harigaya, and T. Nakamura, "Development of a peristaltic crawling robot for long-distance inspection of sewer pipes," in *IEEE/ASME Trans. Mechatron.*, Jul 2014, pp. 1552–1557.

[3] Y. Zhang, M. Zhang, H. Sun, and Q. Jia, "Design and motion analysis of a flexible squirm pipe robot," in *2010 International Conference on Intelligent System Design and Engineering Application (ISDEA)*, vol. 1, 2010, pp. 527–531.

[4] J. Zuo, G. Yan, and Z. Gao, "A micro creeping robot for colonoscopy based on the earthworm," *Journal of Medical Engineering & Technology*, vol. 29, no. 1, pp. 1–7, 2005.

[5] R. Das, S. P. M. Babu, F. Visentin, S. Palagi, and B. Mazzolai, "An earthworm-like modular soft robot for locomotion in multi-terrain environments," *Scientific Reports*, vol. 13, no. 1, 2023.

[6] Y. Peng, H. Nabae, Y. Funabora, and K. Suzumori, "Controlling a peristaltic robot inspired by inchworms," *Biomimetic Intelligence and Robotics*, vol. 4, no. 1, 2024.

[7] L. Shui, L. Zhu, Z. Yang, Y. Liu, and X. Chen, "Energy efficiency of mobile soft robots," *Soft Matter*, vol. 13, no. 44, pp. 8223–8233, 2017.

[8] Y. Murakami, H. Uchiyama, J. Kurata, and M. Maeda, "Dynamical locomotion analysis and a model for the peristaltic motion of earthworms," *2006 SICE-ICASE International Joint Conference*, pp. 4224–4229, 2006.

[9] H. Omori, T. Hayakawa, and T. Nakamura, "Locomotion and turning patterns of a peristaltic crawling earthworm robot composed of flexible units," in *2008 IEEE/RSJ International Conference on Intelligent Robots and Systems (IROS)*, 2008, pp. 1630–1635.

[10] Y. Tanaka, K. Ito, T. Nakagaki, and R. Kobayashi, "Mechanics of peristaltic locomotion and role of anchoring," *Journal of the Royal Society Interface*, vol. 9, no. 67, pp. 222–233, 2012.

[11] K. Zimmermann and I. Zeidi, "Worm-like locomotion as a problem of nonlinear dynamics," *J. Theoret. Appl. Mech.*, vol. 45, pp. 179–187.

[12] Y. Shen, N. E. Leonard, B. Bamieh, and J. Arbelaiz, "Optimal gait design for nonlinear soft robotic crawlers," *IEEE Control Systems Letters*, vol. 8, pp. 3141–3146, 2024.

[13] Q. Xu, W. Fan, Y. Luo, S. Wang, and H. Jiang, "Nonlinear effect of forced harmonic oscillator subject to sliding friction and simulation by a simple nonlinear circuit," *American Journal of Physics*, vol. 87, no. 2, pp. 116–124, 2019.

[14] C. Hatipoglu and U. Ozguner, "Robust control of systems involving non-smooth nonlinearities using modified sliding manifolds," in *Proceedings of the 1998 American Control Conference (ACC)*, vol. 4, Philadelphia, PA, USA, 1998, p. 2133.

[15] A. S, S. A, and B. S, "Friction models for sliding dry, boundary and mixed lubricated contacts," *Special issue on NORDTRIB*, vol. 40, no. 4, pp. 580–587, 2007.

[16] P. Paoletti and L. Mahadevan, "A proprioceptive neuromechanical theory of crawling," *Proceedings of the Royal Society B: Biological Sciences*, vol. 281, no. 1790, p. 20141092, 2014.

[17] M. Calisti, G. Picardi, and C. Laschi, "Fundamentals of soft robot locomotion," *Journal of the Royal Society Interface*, vol. 14, no. 130, p. 20170101, 2017.

[18] R. McNeill Alexander, *Climbing, Jumping, and Crawling*. New York, NY/Oxford, UK: Freeman and Company, 1992.

[19] A. D. H. et al., "Peristaltic locomotion of a modular mesh-based worm robot: Precision, compliance, and friction," *Soft Robotics*, vol. 2, no. 4, pp. 135–145, 2015.

[20] M. H. Holmes, *Introduction to Perturbation Methods*. New York, NY, USA: Springer, 2013.

[21] A. H. Nayfeh, *Perturbation Methods*. New York, NY, USA: Wiley, 1973.

[22] S. U. W. Gilpin and C. P. Brangwynne, "Worms under pressure: Bulk mechanical properties of c. elegans are independent of the cuticle," *Biophysical Journal*, vol. 108, no. 8, pp. 1887–1898, Apr 2015.

APPENDIX I
DERIVATION OF CRAWLER DYNAMICS

The net force acting on a cross-section (Fig. 1) is the sum of the force experiences by each respective side of the section.

$$\frac{\delta T_{\text{elastic}}}{\delta x} = A_c E \frac{u'-u}{(\delta x)^2}\ , \quad \frac{\delta T_{\text{muscle}}}{\delta x} = A_m \frac{f'-f}{\delta x}$$
$$\frac{F_{\text{friction}}}{\delta x} = \frac{1}{\delta x}\int_0^{\delta x} F\left(\frac{\partial u}{\partial t}\right) dx\ , \quad \frac{F_{\text{inertial}}}{\delta x} = \frac{1}{\delta x}\int_0^{\delta x} \rho \frac{\partial^2 u}{\partial t^2} dx$$

Taking the continuum limit as $\delta x \to 0$ yields,

$$\lim_{\delta x\to 0} A_c E \frac{u'-u}{(\delta x)^2} = A_c E \frac{\partial^2 u}{\partial x^2},\ \lim_{\delta x\to 0} A_m \frac{f'-f}{\delta x} = A_m \frac{\partial f}{\partial x}$$
$$\lim_{\delta x\to 0} \frac{1}{\delta x}\int_0^{\delta x} \rho \frac{\partial^2 u}{\partial t^2} + F\left(\frac{\partial u}{\partial t}\right) dx = \rho \frac{\partial^2 u}{\partial t^2} + F(\frac{\partial u}{\partial t})$$

Applying Newton's second law per unit length gives (14).

APPENDIX II
PROOF OF PROPOSITION 1

We solve (25) by assuming traveling wave solutions of the form $\tilde{\mu}^{(0)}(\chi - \alpha\tau_1)$ to obtain

$$\tilde{\mu}^{(0)}(\chi, \tau_1, \tau_2) = R_0 \cos(\chi - \alpha\tau_1 - \phi_0) + C_0\tau_2, \qquad (38)$$

Where $C_0 = \frac{\pi_r n_F}{\zeta}$ is included to satisfy the solvability condition (Lemma 1) at $O(\epsilon)$ with $\mathcal{L}^\dagger = (\partial_{\chi\chi} - \partial_{\tau_1\tau_1} + \zeta\partial_{\tau_1})$. It can easily be verified that the $-\pi_r n_F$ term in (23) must be eliminated to satisfy the solvability condition and avoid secular growth in $\tilde{\mu}^{(1)}$, so we choose C_0 to eliminate this term. Substituting (38) into (26) yields,

$$\mathcal{L}\tilde{\mu}^{(1)} = \pi_r \operatorname{sgn}\left[R_0\alpha \sin\xi + \epsilon C_0\right] \qquad (39)$$

Where $\xi = \chi - \alpha\tau_1 - \phi_0$ is the traveling coordinate. The nonhomogeneous term in (39) is a traveling square wave which can be represented as Fourier series:

$$\mathcal{L}\mu^{(1)} = \frac{2\gamma}{\pi} + \sum_{n=1}^{\infty} a_n \cos(n\xi) + b_n \sin(n\xi), \qquad (40)$$

where $\gamma = \sin^{-1}(\frac{\epsilon C_0}{R_0\alpha})$, $a_n = \frac{2}{\pi n}(\sin(n(\gamma+\pi)) + \sin(n\gamma))$, and $b_n = \frac{2}{\pi n}(\cos(n\gamma) - \cos(n(\gamma+\pi)))$. The DC term, $2\gamma/\pi$, and the $\partial_{\tau_1}\tilde{\mu}^{(1)}$ terms in (40) again lead to a secular term in $\tilde{\mu}^{(1)}$. Thus, we update $\tilde{\mu}^{(0)}$ to the expression in (27) to satisfy the new solvability condition.

This updated term $\tilde{\mu}_\tau^{(0)}$ can be substituted into in (26) to obtain a new solvability condition which improves the approximation of the linear drift of the crawler. For our purposes, the approximated solutions in (27) and (28) agree strongly with numerical solutions to the full dynamics given in (14) (see Fig. 4). Thus, we proceed by solving,

$$\mathcal{L}\mu^{(1)} = \sum_{n=1}^{\infty} a_n \cos(n\xi) + b_n \sin(n\xi), \qquad (41)$$

which suggests a trial solution of the form (28). Substituting this expression into (41) and matching coefficients provides the values of R_n and ϕ_n specified in (29).